Journal of ELECTRONIC MATERIALS, Vol. 46, No. 10, 2017
DOI: 10.1007/s11664-017-5600-z

The Investigation of Electronic, Elastic and Vibrational Properties of an Interlanthanide Perovskite: $PrYbO_3$

CAGIL KADEROGLU,[1,6] GOKHAN SURUCU,[2,3,4] and AYTAC ERKISI[5]

1.—Department of Physics Engineering, Ankara University, 06100 Ankara, Turkey. 2.—Department of Electric and Energy, Ahi Evran University, 40100 Kirsehir, Turkey. 3.—Department of Physics, Middle East Technical University, 06800 Ankara, Turkey. 4.—Photonics Application and Research Center, Gazi University, 06500 Ankara, Turkey. 5.—Department of Physics Engineering, Hacettepe University, 06800 Ankara, Turkey. 6.—e-mail: cagil.kaderoglu@eng.ankara.edu.tr

The structural, mechanical, electronic and lattice dynamical properties of the $PrYbO_3$ compound from the ABO_3-type perovskite family have been investigated by performing the first-principles density functional theory calculations using the generalized-gradient approximation (GGA) with corrected Coulomb interactions (GGA+U). Structural parameters, formation energies and phase transition pressures for the five possible phases of this compound have been calculated. Then, the spin-dependent electronic band structure and corresponding density of states (DOS) have been plotted. Also, the shear modulus, Young's modulus, Poisson's ratio, G/B ratio, hardness and anisotropy factors have been calculated to investigate mechanical behavior of this material. Furthermore, the phonon dispersion curves have also been plotted as corresponding phonon PDOS. According to our calculations, the orthorhombic phase of the five phases of $PrYbO_3$ is the most stable one and exhibits a half-metallic character, which can therefore be a candidate for spintronic applications.

Key words: Perovskites, *ab initio*, elasticity, mechanical properties, phonon, band calculations, half metals

INTRODUCTION

Since its first discovery in 1839, perovskite ($CaTiO_3$) and perovskite-like structures have drawn a considerable amount of research interest because of their importance for technological applications due to the structural, electronic, magnetic and optical properties they exhibit.[1–7]

A common formula of the perovskite structure can be generalized as ABX_3, where the A and B atoms are cations with a remarkable size difference, as $A > B$, while the X atom is an anion which is known to be oxygen (O) and halogens in naturally occurring perovskites and synthetic compounds, respectively.[8] Oxides of perovskites accordingly have the formula of ABO_3, and are ideally formed in cubic structure with A atoms at the corners, B atoms in the body center and O atoms on the face centers. In most cases, due to the mismatch in the cations' sizes, a structural distortion occurs leading to this ideal cubic structure to transforming into a low-symmetry orthorhombic or tetragonal structure by reducing the coordination numbers of cations and tilting the oxygen octahedra.[1,5,9] This structural phase transformation results in significant effects on the electrical properties of the material, thus putting the perovskite-type oxides in the center of ferro/anti-ferroelectric and high-K dielectric applications.[9–12] Also, these oxides are key elements of colossal magnetoresistance, positive temperature coefficient (PTC) thermistor and battery material industries as well as smart and superconducting devices.[5,13] In addition to the above-mentioned properties, perovskite oxides are used as photocatalysts for water splitting and electrodes for

(Received January 24, 2017; accepted May 17, 2017; published online May 30, 2017)

electrochemical reduction of nitrous oxide which are both important for environmental pollution control.[14,15]

Lanthanide-based perovskites, whose *A* and *B* sites are occupied by a lanthanide and a transition element, respectively, are an important sub-group of perovskite oxides. On the other hand, the physical properties of the ABO_3 perovskites are generally determined by the *B* cation of the compound.[16] In this context, it is important to investigate all possible candidates for the *B* position to improve the tunable optical, electrical and magnetic properties of these materials demanded by the downscaling of devices. In this case, interlanthanide perovskite oxides, alias ternary lanthanide oxides, constitute an important step of the research. In general, $RERE'O_3$ compounds, where *RE* is the larger element from the left side of the lanthanide series while *RE′* is the smaller one from the opposite side, are the key materials for the protonic conductor and scintillator studies[17] as well as some optical[18,19] and microwave applications.[20,21] Regarding the above-stated properties, thorough investigation of $RERE'O_3$ perovskites has a great importance in order to increase their potential usage in advanced technology.

$PrYbO_3$ is an important member of the interlanthanide oxides group when considering how the number of the elements in this group is small. However, only a few studies about it can be found in the literature.[9,16,22,23] In the experimental studies carried out by Berndt et al.,[22] Coutures et al.,[23] and Ito et al.,[16] $PrYbO_3$ was prepared by solid-state reactions, confusion techniques and coprecipitation methods to examine the thermal stability, optical properties and magnetic susceptibility of this compound, respectively. On the other hand, there is only one theoretical work in the literature carried out by Coh et al., in which only the structural and dielectric parameters of $PrYbO_3$ were calculated by using density functional theory (DFT) as implemented in the Quantum-Espresso package.[24]

Differently from these previous works, in this study, we have carried out a very detailed *ab initio* analysis of the $PrYbO_3$ compound by using the Vienna *Ab Initio* Simulation Package (VASP) code. In this context, five different ferromagnetic phases, crystallized in orthorhombic, tetragonal, rhombohedral, hexagonal and cubic structures, have been considered to make an in-depth structural analysis. The elastic properties of any material are as important as its magnetic and electronic properties when deciding the suitability of the material for a specific application, due to its information content about the nature of the binding forces and the thermal properties.[25] Thus, elastic parameters have been calculated to reveal the mechanical properties of the material such as stability, hardness and stiffness which are important especially for thin film applications.[26–28] Moreover, the electronic band structure and corresponding density of states (DOS) have been plotted as well as phonon dispersion curves. To the extent that we know, these detailed calculations have not been carried out before for the $PrYbO_3$ compound.

METHODOLOGY

First-principles DFT calculations herein were carried out by using the VASP software.[29,30] The projector augmented wave approach[31] was applied to describe the electron–ion interaction in a plane wave basis with a 800-eV cut-off energy which is large enough for a precise determination of the physical properties. The exchange–correlation functional was calculated with the Perdew–Burke–Ernzerhof[32] pseudopotentials under the GGA with a supplement of a Hubbard+U correction using Dudarev's approach[33] for the on-site Coulomb interactions of the f states of the Pr and Yb atoms, where U_{eff} is here 6.0 eV. The Brillouin zone integration was carried out using an automatically generated $10 \times 10 \times 10$ Monkhorst–Pack[34] *k*-point grid for the cubic and tetragonal phases, with $10 \times 10 \times 6$, $10 \times 10 \times 8$ and $6 \times 4 \times 6$ *k*-point meshes for the hexagonal, rhombohedral and orthorhombic phases, respectively. The quasi-Newton method was used to relax ions into their ground-state positions until all the forces were smaller than 10^{-5} eV $Å^{-1}$. The energy tolerance was less than 10^{-9} eV per unit cell in the iterative solution of the Kohn–Sham equations. Cell volume was also allowed to relax. Partial occupancies were calculated using Gaussian-type smearing with a width of 0.01 eV.

The crystal structure of the $PrYbO_3$ alloy in cubic (Pm-3m) and tetragonal (P4mm) phases with 5-atom primitive cells, rhombohedral (R-3c) phase with a 10-atom primitive cell, hexagonal ($P6_3/mmc$) and orthorhombic (Pbnm) phases with 20-atom primitive cells are presented in Fig. 1a–e, respectively.

RESULTS AND DISCUSSION

Structural and Electronic Properties

In this work, the $PrYbO_3$ compound has been modeled in five different crystal systems, namely orthorhombic (Fig. 1a), tetragonal (Fig. 1b), rhombohedral (Fig. 1c), hexagonal (Fig. 1d) and cubic (Fig. 1e) phases. The lattice geometries and ionic positions of each considered crystal have been fully optimized to obtain fully relaxed structures in order to determine the most stable one among these five phases. Based upon this structural optimization, formation enthalpies (ΔH_f) of the corresponding crystals have been calculated and tabulated in Table I. Since the enthalpy of formation can be approximately calculated from internal energy changes,[35] the ΔH_f results here have been obtained according to the following formula (1), where E_t is the total energy of the compound.

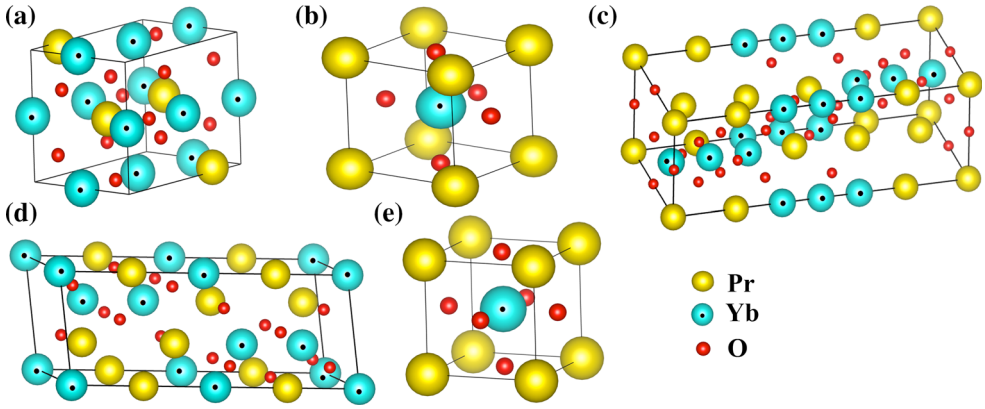

Fig. 1. The crystal structure of $PrYbO_3$ in: (a) orthorhombic Pbnm space group, (b) tetragonal P4mm space group, (c) rhombohedral R-3c space group, (d) hexagonal $P6_3/mmc$ space group, (e) cubic Pm-3m space group.

Table I. The calculated equilibrium lattice parameters (*a*, *b* and *c* in Å), formation energies (ΔH_f in eV/atom), and atomic positions for $PrYbO_3$ compound (*T* and *E* indicate the theoretical and experimental results, respectively)

$PrYbO_3$	*a*	*b*	*c*	ΔH_f	Atomic positions
Orthorhombic (Pbnm)	5.810	6.021	8.771	−23.862	Pr: 4c (0.439, 0.25, 0.034)
	T[9] 5.8085	6.0544	8.4481		Yb: 4b (0.5, 0.0, 0.0)
	E[16] 5.7684	5.9929	8.3547		O_1: 4c (0.066, 0.25, 0.854)
	E[22] 5.776	5.995	8.368		O_2: 8d (0.203, 0.008, 0.296)
Tetragonal (P4mm)	4.115	–	4.113	−21.576	Pr: 1a (0.0, 0.0, 0.080)
					Yb: 1b (0.5, 0.5, 0.580)
					O_1: 1b (0.5, 0.5, 0.080)
					O_2: 2c (0.5, 0.0, 0.579)
Rhombohedral (R-3c)	6.048	6.048	6.048	−23.769	Pr: 6b (0.0, 0.0, 0.0)
					Yb: 6a (0.0, 0.0, 0.25)
					O: 18e (0.532, 0.0, 0.25)
Hexagonal ($P6_3/mmc$)	5.695	–	9.501	−21.655	Pr_1: 2a (0.0, 0.0, 0.0)
					Pr_2: 2c (0.333, 0.667, 0.25)
					Yb: 4f (0.333, 0.667, 0.6246)
					O_1: 6g (0.5, 0.0, 0.0)
					O_2: 6h (0.86, 0.72, 0.25)
Cubic (Pm-3m)		–	–	−21.578	Pr: 1b (0.5, 0.5, 0.5)
					Yb: 1a (0.0, 0.0, 0.0)
	4.115				O: 3d (0.5, 0.0, 0.0)

$$\Delta H_f = E_t(\mathrm{Pr\,YbO_3}) - [E_t(\mathrm{Pr}) + E_t(\mathrm{Yb}) + 3E_t(\mathrm{O})] \quad (1)$$

The energy of the oxygen has been calculated by using a monoclinic alpha-oxygen model (space group: C2/m) including spin-polarization.[35,36] The negative values of the formation energies in Table I indicate that all crystal phases are structurally stable and synthesizable, but the orthorhombic (Pbnm) phase is the most stable one with the lowest ΔH_f value.

To cross-check this result, we have calculated the Goldschmidt tolerance factor (t_{IR})[37] which is a geometric parameter describing the structural stability of the perovskite material as a function of the ionic radii of the components as given in the formula (2);

$$t_{IR} = \frac{r(\mathrm{Pr}^{3+}) + r(\mathrm{O}^{2-})}{\sqrt{2}\left(r(\mathrm{Yb}^{3+}) + r(\mathrm{O}^{2-})\right)} \quad (2)$$

$0.9 < t_{IR} < 1.0$ indicates a good fit into the ideal cubic structure while $0.71 < t_{IR} < 0.9$ results in a distorted perovskite structure with a space group symmetry change from cubic to orthorhombic.[9,38,39] Using the ionic radii given by Shannon,[40] the ionic radii calculated tolerance factor of $PrYbO_3$ has been found as 0.847 which confirms our ΔH_f result. This value is also consistent with the value of 0.843 which has been previously given in Ref. 16 as the

minimum required tolerance factor to prepare the $PrYbO_3$. The same result can also be verified by the bond valence-based tolerance factor of $PrYbO_3$ (t_{BV} = 0.844), in which bond distances are employed instead of ionic radii summation, and the linear correlation between t_{IR} and t_{BV} can be described by the equation $t_{BV} = 1.015t_{IR} - 0.015$.[41]

To visualize the above-stated case in detail, energy–volume graphics have been plotted in Fig. 2. Here, the $PrYbO_3$ compound shows energetically similar behavior in both cubic and tetragonal phases and also seems to be the most unstable in both of these structural phases with only a slightly higher energy than the hexagonal one. The orthorhombic phase (Pbnm) is the most stable for the $PrYbO_3$ compound with a slightly lower energy than the rhombohedral phase. The calculated equilibrium lattice parameters and atomic positions of these five phases are also tabulated in Table I, from it can be seen that the available theoretical and experimental data in the literature for the most stable orthorhombic phase are consistent with the calculated ones here.

Subsequent to the stability calculations, phase transition pressures have been obtained by plotting enthalpy–pressure graphics as seen in Fig. 3. At zero pressure, the enthalpy of the $PrYbO_3$ compound in the orthorhombic phase (Pbnm) is the minimum, as expected. The enthalpies of the cubic, tetragonal and hexagonal phases are equal at the pressure of −3.924 GPa. Also, the enthalpies of the rhombohedral and orthorhombic phases become equal at −2.700 GPa and the enthalpies of the rhombohedral and hexagonal phases become equal at 44.091 GPa. The negative values of pressure correspond to extended lattices. It is clearly seen that there is a phase transformation between the rhombohedral and hexagonal phases while the most stable orthorhombic phase remains stable in a wide range of positive pressures.

To discover the electronic nature of $PrYbO_3$, we have calculated the spin-dependent energy bands of the five phases along the high-symmetry directions in the Brillouin zone. The calculated energy band gaps of the spin-up and spin-down states are given in Table II, from which it can be seen that both the spin-up and spin-down states of the tetragonal, rhombohedral and cubic phases are almost metallic with band gaps smaller than 0.02 eV which is a negligible value. While the spin-down states of the orthorhombic and hexagonal phases resemble others, the spin-up states of these two structures have significant band gaps. Therefore, these two phases of $PrYbO_3$ can be assumed to show a half-metallic character. Also, the calculated total magnetic moments of these phases are $\mu_{orthorhombic}$ = 4.06 and $\mu_{hexagonal}$ = 0.2, which are very close to integer values as a typical property of half-metals.[42,43] Thus, it is clearly seen that these two phases are suitable for applications in spintronics, as previously mentioned for similar materials in Refs. 42, 44, 45 due to their ferromagnetic and half-metallic behavior. To see the details of the electronic structure, we have plotted the energy band graphics and the DOS of the most stable orthorhombic phase. In Fig. 4, the Fermi level (E_f) shown by a broken horizontal line intersects the $E(k)$ curves in the minority (down)-spin state causing the above-mentioned metallic behavior. In contrast, there is a direct band gap of 4.915 eV at the Γ-point in the majority (up)-spin state that leads to insulator behavior.

Elastic Properties

Elastic constants are the key parameters when identifying a material's mechanical and dynamical

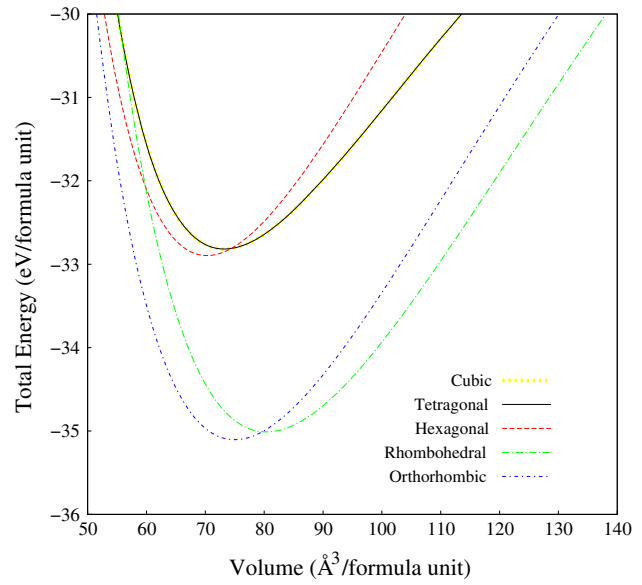

Fig. 2. Total energies as a function of volume for the considered phases of $PrYbO_3$.

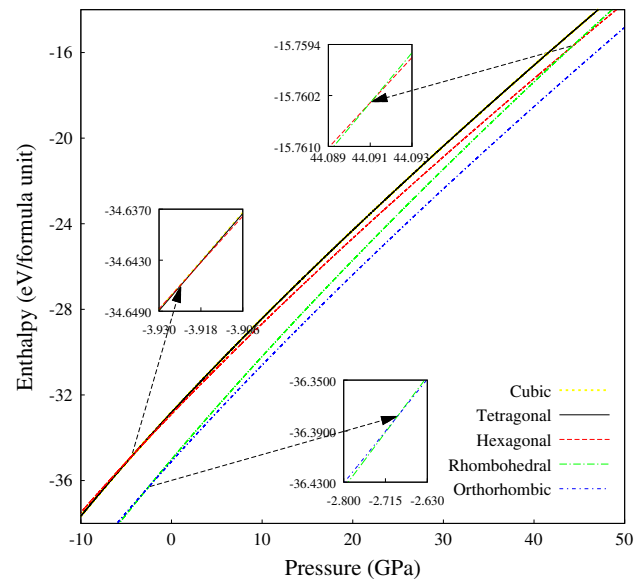

Fig. 3. Enthalpies as a function of pressure for the considered phases of $PrYbO_3$.

Table II. The calculated energy band gaps (E_{gap} in eV) of $PrYbO_3$ for all phases

	Pbnm	P4mm	R-3c	$P6_3/mmc$	Pm-3m
Majority (up)	4.915	0.001	0.001	2.789	0.016
Minority (down)	–	0.011	0.000	0.000	0.008

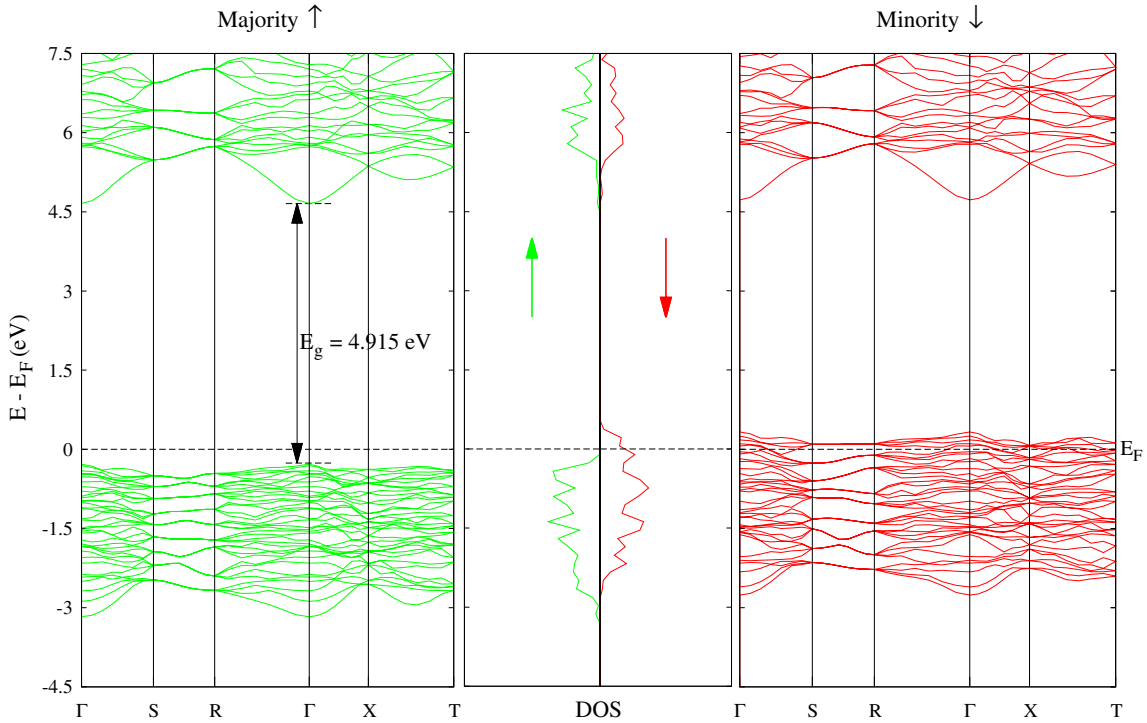

Fig. 4. The electronic band structure and the corresponding DOS graphics of the orthorhombic $PrYbO_3$.

Table III. The calculated elastic constants (C_{ij}, in GPa) of $PrYbO_3$ for all phases

	Pbnm	P4mm	R-3c	$P6_3/mmc$	Pm-3m
C_{11}	190.1	165.0	155.7	171.1	148.7
C_{12}	95.2	84.2	74.8	87.0	95.5
C_{13}	84.7	110.0	62.9	89.4	
C_{14}			−3.1		
C_{22}	122.8				
C_{23}	86.2				
C_{33}	202.5	114.5	118.9	185.9	
C_{44}	52.5	37.0	30.8	13.0	36.5
C_{55}	50.0				
C_{66}	51.6	37.0		42.1	

behavior which are important to know for any technological application. The stress–strain method-implemented *ab initio* calculations can be used to obtain these constants to reveal the information they have about the stability, hardness and stiffness of the material. The calculated elastic constants of the five considered phases are given in Table III.

The mechanical stability of a crystal, in other words the durability of the crystal against external forces, is a desirable property in order to ensure its sustainability in any application. Mechanical stability is determined according to the Born-Huang criteria[46] which differ for each crystal system and must be satisfied by the elastic constants of the crystal. Starting from this point, the elastic

constants given in Table III have been first used to determine the mechanical stability of the five considered phases using the criteria given in Ref. 46. Our results satisfy these stability conditions, suggesting that all possible crystal structures of $PrYbO_3$ are mechanically stable.

Second, these constants have been used to calculate the bulk and shear moduli according to the Voigt–Reuss–Hill approximations.[47–49] Here, the Voigt bound is the upper limit of the moduli assuming a uniform strain throughout the crystal while the Reuss bound is the lower limit of the moduli with the assumption of uniform stress. As for the Hill approximation, it is widely used to make acceptable estimations of elastic parameters for polycrystalline materials using the arithmetic mean of the Voigt and Reuss limits as seen in formula (3):

$$\begin{aligned} \mathrm{B} &= (B_\mathrm{V} + B_\mathrm{R})/2 \\ G &= (G_\mathrm{V} + G_\mathrm{R})/2 \end{aligned} \tag{3}$$

Here, subscripts V and R symbolize the Voigt and Reuss bounds, respectively, and the detailed formulas of these bounds for each type of crystal structure derived from their own elastic constants can be also found in Ref. 46. Moreover, Young's modulus (E) and Poisson's ratio (v) have been derived from the above-mentioned B and G values using the following relationships:

$$\begin{aligned} E &= 9BG/(3B + G) \\ v &= (3B - 2G)/[2(3B + G)] \end{aligned} \tag{4}$$

The calculated bulk moduli (B), shear moduli (G), Young's moduli (E), Poisson's ratio (v), Pugh's modulus (G/B) and Vickers hardness (H_V) for the five phases of $PrYbO_3$ are listed in Table IV.

The bulk modulus measures how a material resists volume change without a shape deformation when subjected to hydrostatic pressure. In other words, it characterizes the incompressibility property of the material. The shear modulus is a measurement of resistance to transverse deformations, namely to shape change at constant volume. It is defined as the ratio of shear stress to shear strain and depends on both the plane and the direction. In general, a high value of shear modulus is mainly due to directional bonding between atoms where the electron density is geometrically localized and thus more energy is needed to break these bonds and the material is assumed to be more rigid.[50,51] As seen in Table IV, the rhombohedral phase is the most compressible one with the smallest bulk modulus of 91.1 GPa while the others have a\ larger bulk modulus (>110 GPa) without a significant difference between them. In addition, the tetragonal phase has the smallest shear modulus value of 25.1 GPa. The orthorhombic phase, as the most stable, has a bulk modulus of 113.2 GPa and a shear modulus of 45.3 GPa which is the highest value in the table. But these values are still smaller when compared to other lanthanide-based Pbnm perovskites in the literature.[39,52] The orthorhombic phase also has the highest Young's modulus (119.9 GPa) which is used to provide a measure of the stiffness of the solid. Thus, according to the bulk, shear and and Young's moduli results, it can be said that the orthorhombic phase of the $PrYbO_3$ is the most rigid and stiffest among the other calculated phases.

Both the Poisson's ratio and Pugh's modulus can be used to determine the bonding nature of the crystal. The typical value of v is about 0.1 for covalent materials while 0.25 corresponds to the ionic materials. On the other hand, if the value of the G/B ratio is about 1.1, covalent bonding is more dominant than ionic bonding while the opposite is valid in the $G/B \approx 0.6$ case.[53] In addition, v and G/B values can also be used to determine the ductility or brittleness of a material. According to Frantsevich's rule, $v = 0.33$ is the critical value of Poisson's ratio where larger values refer to ductility while lower values indicate brittleness.[54] Also, according to Pugh's criteria, $G/B > 0.5$ indicates brittleness, otherwise the material is assumed to be ductile.[55,56] In the light of our results in Table IV, it can be said that all the phases of $PrYbO_3$ have both ionic and ductile characters.

Hardness values of the material have been calculated by using a semi-empirical method based on Pugh's modulus ratio developed by Chen et al.[57] It is given as;

$$H_\mathrm{V} = 2\left(k^2 G\right)^{0.585} - 3;\ (k = G/B) \tag{5}$$

According to the H_V values in Table IV, all the phases are relatively soft. The hardest phase among them is the orthorhombic with $H_\mathrm{V} = 5$ GPa, while the tetragonal phase has the lowest hardness value. These values are in the range of the reported values

Table IV. The calculated bulk modulus (B in GPa), shear moduli (G in GPa), Young's modulus (E in GPa), Poisson's ratio (v), Pugh's modulus (G/B) and Vickers hardness (H_v in GPa) for the $PrYbO_3$ compound

Phases	B	G	E	K	G/B	H_v
(Pbnm)	113.2	45.3	119.9	0.32	0.40	5.0
(P4mm)	115.2	25.1	70.2	0.39	0.22	2.7
(R-3c)	91.1	31.6	84.9	0.34	0.35	3.6
($P6_3/mmc$)	117.6	26.7	74.4	0.39	0.23	3.1
(Pm-3m)	113.2	32.1	87.9	0.37	0.28	3.5

in the literature for some other lanthanide-based perovskites.[58–60]

The anisotropy of elasticity has an important role in determining the technological application of the material due to its effects on the physical/mechanical properties such as unusual phonon modes, phase transformations, precipitation, dislocation dynamics, anisotropic plastic deformation, etc. as mentioned in Ref. 61. Also, the formation of microcracks, which is important to understand in order to improve the mechanical durability of the material in any application, is due to the significant elastic anisotropy.[62] Therefore, anisotropy calculations are necessary to make a complete elastic analysis of the

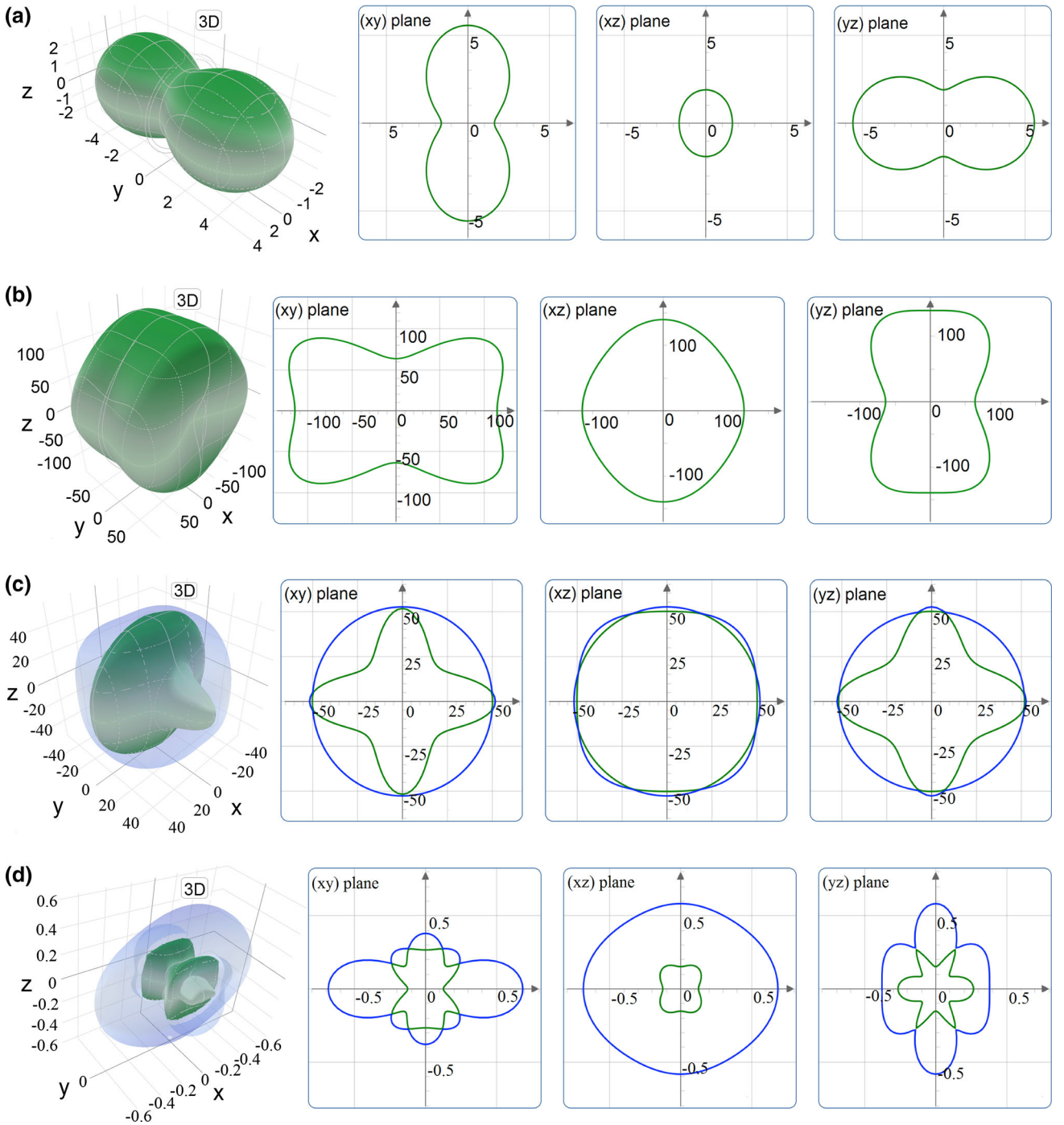

Fig. 5. The calculated directional dependence of the mechanical properties; (a) compressibility, (b) Young's modulus, (c) shear modulus, (d) Poisson's ratio.

material. Here, the ElAM code[63] has been used to calculate and visualize the directional dependence of the linear compressibility, Young's modulus, the shear modulus, and Poisson's ratio. In the graphics of these physical properties, the deviation from the spherical shape indicates the degree of anisotropy. Three-dimensional (3D) dependence of these parameters along the crystallographic directions and their 2D projections on the three planes has been given in Fig. 5a–d for the most stable orthorhombic phase. According to the figure, all the parameters possess obvious anisotropy as follows: linear compressibility (Fig. 5a) has the minimum in the y-axes while it has its maximum in the x- and z-axes. Also it is isotropic in the x–z plane. In the x–y plane, Young's modulus (Fig. 5b) has its maximum when it deviates from the axes at an angle of 35°. The deviation of it from the spherical shape is much more less in x–z plane. In the y–z plane, it has its maximum on the y-axes while the minimum value sits on the z-axes. For the shear modulus (Fig. 5c), it has the maximum values on the axes in both the x–y and y–z planes while it becomes smaller with a 45° deviation from these axes. Also, it seems isotropic in the x–z plane. A more complicated anisotropy is seen for Poisson's ratio (Fig. 5d) in the y–z plane. There is also no isotropic behavior of v in the rest of the planes. The maximum and minimum values of these parameters are tabulated in Table V.

Vibrational Properties

The present phonon frequencies in the orthorhombic (Pbnm) phase have been calculated by the PHONOPY code[64] using the inter-atomic force constants obtained from VASP 5.3.5. In the PHONOPY code, force constant matrices and phonon frequencies are calculated by using the

Table V. Maximum and minimum values of Young's modulus (E_{max} and E_{min}, in GPa), linear compressibility (β_{max} and β_{min}, TPa^{-1}), shear moduli (G_{max} and G_{min}, in GPa), and Poisson's ratio (v_{max} and v_{min}) of the $PrYbO_3$ compound

Phases	Young's modulus		Linear compression		Shear modulus		Poisson ratio	
	E_{min}	E_{max}	β_{min}	β_{max}	G_{min}	G_{max}	v_{min}	v_{max}
Pbnm	63.49	144.83	1.64	5.54	1.0	55.84	0.13	0.69
P4mm	17.39	103.25	1.04	6.74	1.0	40.40	−0.36	1.31
R-3c	82.20	108.34	2.87	5.37	1.0	40.45	0.26	0.39
$P6_3/mmc$	45.32	123.97	2.48	3.02	1.0	44.41	0.13	0.74
Pm-3m	74.01	98.87	2.94	2.94	1.0	36.50	0.25	0.48

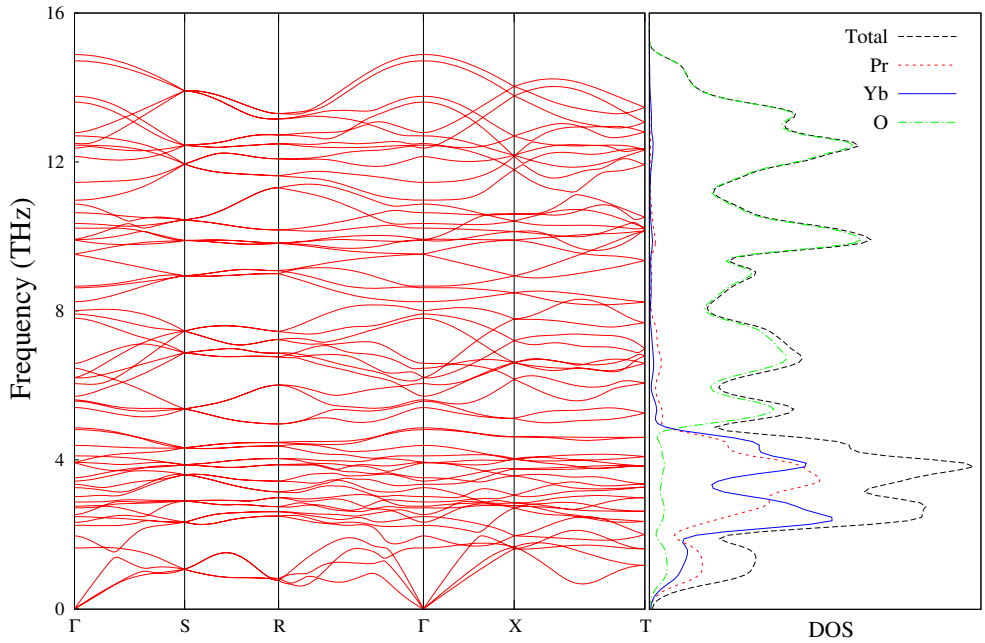

Fig. 6. Phonon dispersion curves and partial PDOS of the orthorhombic $PrYbO_3$.

"Linear Response Method" within the density functional perturbation theory[64–67] for a real space supercell. The phonon dispersion curves along the high symmetry directions and the corresponding phonon DOS plotted for a $2 \times 2 \times 1$ supercell can be seen in Fig. 6. Due to having 20 atoms in the primitive cell, there are 60 branches in the phonon graph consisting of 3 acoustic and 57 optic branches. The sharp peaks in the phonon DOS correspond to the flat modes of the phonon dispersion curves. When analysing these two graphics together, it can be seen that the main contribution to the acoustic branches is due to the Pr and Yb atoms, with Pr especially dominant. The same situation is also valid for the optic branches with frequencies lower than about 5 THz. But here, both of the Pr and Yb atoms seems to contribute almost equally. At the higher frequencies, optic branches mainly arise from the oxygen atoms. In acoustic branches, there is no soft mode and thus orthorhombic $PrYbO_3$ is dynamically stable. Also, no clear gap between the optic and acoustic branches is observed.

CONCLUSION

In this paper, *ab initio* techniques have been used to investigate the structural, mechanical, electronic and vibrational properties of the $PrYbO_3$ compound which is an $A^{3+}B^{3+}O_3$-type interlanthanide perovskite. Five possible structural phases have been included in the calculations and both the structural parameters and formation enthalpies of these phases have been calculated to find the most stable one. Among these considered structures, the energetically most favorable one has been found to be the orthorhombic phase (*Pbnm*).

Spin-dependent energy bands have been calculated for these five phases. According to these calculations, only the spin-up states of the orthorhombic and hexagonal phases have significant band gaps while the rest is metallic. Thus, these two ferromagnetic phases of this material can be recommended as a candidate for applications in spintronics due to their half-metallic character.

In the second section, mechanical properties have been investigated in detail. Our results have shown that $PrYbO_3$ is a soft and ductile material. Also, the orthorhombic phase is the most rigid and stiffest compared with the others. Finally, to see the directional dependence of the elastic properties, anisotropy graphics of the mechanical properties for the most stable phase has been plotted in both 3D and 2D. As can be seen from these graphs, the elasticity of the $PrYbO_3$ is quite anisotropic.

Lastly, phonon curves and corresponding PDOS graphics of the *Pbnm* structure have been plotted to analyze the individual contribution of the atoms to the acoustic and optic mode frequencies. No negative mode has been found, indicating the dynamical stability of this material.

REFERENCES

1. C.J. Rhodes, *Sci. Prog.* 97, 279 (2014).
2. J.F. Mitchell, D.N. Argyriou, A. Berger, K.E. Gray, R. Osborn, and U. Welp, *J. Phys. Chem. B* 105, 10731 (2001).
3. H.R. Wenk and A. Bulakh, *Minerals: Their Constitution and Origin* (New York: Cambridge University Press, 2004), pp. 1–646.
4. A.M. Glazer, *Acta Cryst.* A31, 756 (1975).
5. M.W. Lufaso and P.M. Woodward, *Acta Cryst. B* 57, 725 (2001).
6. Z.L. Wang and Z.C. Kang, *Functional and Smart Materials* (New York: Plenum Press, 1998), pp. 1–514.
7. F.S. Galasso, *Perovskites and High T_c Superconductors* (New York: Gordon&Breach Science Publishers, 1990), pp. 1–294.
8. A.P. Jones, F. Wall, and C.T. Williams, *Rare Earth Minerals: Chemistry, Origin and Ore Deposits* (Netherlands: Springer, 1996), pp. 1–372.
9. S. Coh, T. Heeg, J.H. Haeni, M.D. Biegalski, J. Lettieri, L.F. Edge, K.E. O'Brien, M. Bernhagen, P. Reiche, R. Uecker, S. Trolier-McKinstry, D.G. Schlom, and D. Vanderbilt, *Phys. Rev. B* 82, 064101 (2010).
10. S. Saha, T.P. Sinha, and A. Mookerjee, *Phys. Rev. B* 62, 8828 (2000).
11. O. Auciello, J.F. Scott, and R. Ramesh, *Phys. Today* 51, 22 (1998).
12. N.A. Hill, *J. Phys. Chem. B* 104, 6694 (2000).
13. C. Li, K.C.K. Soh, and P. Wu, *J. Alloys Compd.* 372, 40 (2004).
14. K.K. Hansen, *Mater. Res. Bull.* 45, 1334 (2010).
15. J. Shi and L. Guo, *Prog. Nat. Sci.* 22, 592 (2012).
16. K. Ito, K. Tezuka, and Y. Hinatsu, *J. Solid State Chem.* 157, 173 (2001).
17. C. Artini, G.A. Costa, M.M. Carnasciali, and R. Masini, *J. Alloys Compd.* 494, 336 (2010).
18. S. Polizzi, S. Bucella, A. Speghini, F. Vetrone, R. Naccache, J.C. Boyer, and J.A. Capobianco, *Chem. Mater.* 16, 1330 (2004).
19. U. Griebner, V. Petrov, K. Petermann, and V. Peters, *Opt. Express* 12, 3125 (2004).
20. R.L. Moreira, A. Feteira, and A. Dias, *J. Phys. Condens. Matter* 17, 2775 (2005).
21. Y. Sharma, S. Sahoo, A.K. Mishra, P. Misra, S.P. Pavunny, A. Dwivedi, S.M. Sharma, and R.S. Katiyar, *J. Appl. Phys.* 117, 094101 (2015).
22. U. Berndt, D. Maier, and C. Keller, *J. Solid State Chem.* 13, 131 (1975).
23. J. Coutures and J.P. Coutures, *J. Solid State Chem.* 19, 29 (1976).
24. P. Giannozzi, S. Baroni, N. Bonini, M. Calandra, R. Car, C. Cavazzoni, D. Ceresoli, G.L. Chiarotti, M. Cococcioni, and I. Dabo, *J. Phys. Condens. Matter* 21, 395502 (2009).
25. J.J.U. Buch, G. Lalitha, T.K. Pathak, N.H. Vasoya, V.K. Lakhani, P.V. Reddy, R. Kumar, and K.B. Modi, *J. Phys. D Appl. Phys.* 41, 025406 (2008).
26. K.A. Pestka II, J.D. Maynard, A. Soukiassian, X.X. Xi, D.G. Schlom, Y. Le Page, M. Bernhagen, P. Reiche, and R. Uecker, *Appl. Phys. Lett.* 92, 111915 (2008).
27. K.A. Pestka II, E.S. Scott, and Y. Le Page, *AIP Adv.* 1, 032154 (2011).
28. C.W. Huang, W. Ren, V.C. Nguyen, Z. Chen, J. Wang, T. Sritharan, and L. Chen, *Adv. Mater.* 24, 4170 (2012).
29. G. Kresse and J. Hafner, *Phys. Rev. B* 47, 558 (1994).
30. G. Kresse and J. Furthmüller, *Comput. Mater. Sci.* 6, 15 (1996).
31. G. Kresse and D. Joubert, *Phys. Rev. B* 59, 1758 (1999).
32. J.P. Perdew, K. Burke, and M. Ernzerhof, *Phys. Rev. Lett.* 77, 3865 (1996).
33. S.L. Dudarev, G.A. Botton, S.Y. Savrasov, C.J. Humphreys, and A.P. Sutton, *Phys. Rev. B* 57, 1505 (1998).
34. H.J. Monkhorst and J.D. Pack, *Phys. Rev. B* 13, 5188 (1976).
35. A. Shigemi and T. Wada, *Jpn. J. Appl. Phys.* 43, 6793 (2004).

36. C.S. Barrett, L. Meyer, and J. Wasserman, *J. Chem. Phys.* 47, 592 (1967).
37. V. Goldschmidt, *Naturwissenschaften* 21, 477 (1926).
38. H. Kronmüller and S. Parkin, eds., *Handbook of Magnetism and Advanced Magnetic Materials,*, vol. 4 Novel Materials (Chichester: Wiley, 2007), pp. 1–1112.
39. A. Erkisi, G. Gokoglu, G. Surucu, R. Ellialtioglu, and E.K. Yildirim, *Philos. Mag.* 96, 2040 (2016).
40. R.D. Shannon, *Acta Cryst.* A32, 751 (1976).
41. H. Zhang, N. Li, K. Li, and D. Xue, *Acta Cryst.* B63, 812 (2007).
42. A. Erkisi, E.K. Yildirim, and G. Gokoglu, *Int. J. Mod. Phys. B* 28/29, 1450205 (2014).
43. Z. Szotek, W.M. Temmerman, A. Svane, L. Petit, P. Strange, G.M. Stocks, D. Kodderitzsch, W. Hergert, and H. Winter, *J. Phys. Condens. Matter* 16, S5587 (2004).
44. A. Abbad, W. Benstaali, H.A. Bentounes, S. Bentata, and Y. Benmalem, *Solid State Commun.* 228, 36 (2016).
45. B. Bouadjemi, S. Bentata, A. Abbad, W. Benstaali, and B. Bouhafs, *Solid State Commun.* 168, 6 (2013).
46. Z. Wu, E. Zhao, H. Xiang, X. Hao, X. Liu, and J. Meng, *Phys. Rev. B* 76, 054115 (2007).
47. W. Voigt, *Lehrbuch der Kristallphysik [The textbook of crystal physics]* (Leipzig: Teubner, 1928), pp. 1–962.
48. A. Reuss, *J. Appl. Math. Mech.* 9, 49 (1929).
49. R. Hill, *Proc. Phys. Soc. A* 65, 349 (1952).
50. J.B. Levine, S.H. Tolbert, and R.B. Kaner, *Adv. Funct. Mater.* 19, 3519 (2009).
51. M.T. Yeung, R. Mohammadi, and Richard B. Kaner, *Annu. Rev. Mater. Res.* 48, 465 (2016).
52. A. Senyshyn, H. Ehrenberg, L. Vasylechko, J.D. Gale, and U. Bismayer, *J. Phys. Condens. Matter* 17, 6217 (2005).
53. J. Haines, J.M. Leger, and G. Bocquillon, *Annu. Rev. Mater. Res.* 31, 1 (2001).
54. N. Frantsevich, F.F. Voronov, and S.A. Bokuta, *Elastic Constants and Elastic Moduli of Metals and Insulators Handbook* (Kiev: Naukova Dumka, 1983), pp. 60–180.
55. U.K. Chowdhury, Md.A. Rahman, Md.A. Rahman, M.T.H. Bhuiyan, and Md.L. Ali, *Cogent Phys.* 3, 1231361 (2016).
56. S.F. Pugh, *Philos. Mag. Ser.* 45, 823 (1954).
57. X.Q. Chen, H. Niu, D. Li, and Y. Li, *Intermetallics* 19, 1275 (2011).
58. S. Yamanaka, K. Kurosaki, T. Maekawa, T. Matsuda, S. Kobayashi, and M. Uno, *J. Nucl. Mater.* 344, 61 (2005).
59. T. Shishido, Y. Zheng, A. Saito, H. Horiuch, K. Kudou, S. Okada, and T. Fukuda, *J. Alloys Compd.* 260, 88 (1997).
60. S. Pathak, S.R. Kalidindi, B. Moser, C. Klemenz, and N. Orlovskaya, *J. Eur. Ceram. Soc.* 28, 2039 (2008).
61. H. Ledbetter and A. Migliori, *J. Appl. Phys.* 100, 063516 (2006).
62. J. Chang, G.P. Zhao, X.L. Zhou, K. Liu, and L.Y. Lu, *J. Appl. Phys.* 112, 083519 (2012).
63. A. Marmier, Z.A.D. Lethbridge, R.I. Walton, C.W. Smith, S.C. Parker, and K.E. Evans, *Comput. Phys. Commun.* 181, 2102 (2010).
64. A. Togo and I. Tanaka, *Scr. Mater.* 108, 1 (2015).
65. S. Baroni, P. Giannozzi, and A. Testa, *Phys. Rev. Lett.* 58, 1861 (1987).
66. X. Gonze and J.P. Vigneron, *Phys. Rev. B* 39, 13120 (1989).
67. X. Gonze, D.C. Allan, and M.P. Teter, *Phys. Rev. Lett.* 68, 3603 (1992).